HUMAN GENE THERAPY 25:199–211 (March 2014)

DOI: 10.1089/hum.2013.152

# Central Nervous System Delivery of Helper-Dependent Canine Adenovirus Corrects Neuropathology and Behavior in Mucopolysaccharidosis Type VII Mice

Lorena Ariza,[1] Lydia Giménez-Llort,[2,*] Aurélie Cubizolle,[3,*] Gemma Pagès,[1] Belén García-Lareu,[1] Nicolas Serratrice,[3] Dan Cots,[1] Rosemary Thwaite,[1] Miguel Chillón,[1,4] Eric J. Kremer,[3] and Assumpció Bosch[1]

**Abstract**

Canine adenovirus type 2 vectors (CAV-2) are promising tools to treat global central nervous system (CNS) disorders because of their preferential transduction of neurons and efficient retrograde axonal transport. Here we tested the potential of a helper-dependent CAV-2 vector expressing $\beta$-glucuronidase (HD-RIGIE) in a mouse model of mucopolysaccharidosis type VII (MPS VII), a lysosomal storage disease caused by deficiency in $\beta$-glucuronidase activity. MPS VII leads to glycosaminoglycan accumulation into enlarged vesicles in peripheral tissues and the CNS, resulting in peripheral and neuronal dysfunction. After intracranial administration of HD-RIGIE, we show long-term expression of $\beta$-glucuronidase that led to correction of neuropathology around the injection site and in distal areas. This phenotypic correction correlated with a decrease in secondary-elevated lysosomal enzyme activity and glycosaminoglycan levels, consistent with global biochemical correction. Moreover, HD-RIGIE-treated mice show significant cognitive improvement. Thus, injections of HD-CAV-2 vectors in the brain allow a global and sustained expression and may have implications for brain therapy in patients with lysosomal storage disease.

## Introduction

Mucopolysaccharidosis type VII (MPS VII or Sly Syndrome) is an autosomal recessive disease that belongs to a group of lysosomal storage disorders (LSD), referred to collectively as mucopolysaccharidoses (MPS), caused by the loss of function of one of several lysosomal enzymes. MPS VII is caused by a deficiency in $\beta$-glucuronidase ($\beta$gluc) activity (EC 3.2.1.31), a lysosomal hydrolase involved in the stepwise degradation of glucuronic acid-containing glycosaminoglycans (GAGs) dermatan sulfate, heparan sulfate, and chondroitin sulfate (Vogler *et al.*, 1994). Lysosomal enzymes are essentially ubiquitously expressed; thus, multiple organs are impaired because of cells accumulating undegraded substrates. MPS VII patients display a range of clinical variability, from the most severe with *hydrops fetalis* to an attenuated phenotype with late onset and almost normal intelligence (Muenzer, 2011). The features of MPS VII include coarse facies, hydrocephaly, and multiple skeletal abnormalities. Affected individuals also frequently develop hepatosplenomegaly, heart valve abnormalities, developmental delay, and progressive intellectual disability (Shipley *et al.*, 1993). The MPS VII mouse has been extensively used as a model of the human LSD as it shares clinical, biochemical, and pathological symptoms, including growth retardation (Birkenmeier *et al.*, 1989; Vogler *et al.*, 1998). Thus, MPS VII mouse is a useful tool for the evaluation of the effectiveness of experimental therapies for MPS VII disorders.

Among the treatments tested for MPS VII, bone marrow transplants, particularly in neonatal mice, can correct widespread lysosomal storage of MPS VII mice in bone, bone marrow, visceral organs, and brain; increase the lifespan to approach that found in normal mice; and correct cardiac abnormalities (Soper *et al.*, 2001; Schuldt *et al.*, 2004). Another therapeutic approach for peripheral LSD symptoms is enzyme replacement therapy (ERT). ERT has improved pathologies in patients with Gaucher disease (Grabowski *et al.*, 1998), Fabry

[1]Center of Animal Biotechnology and Gene Therapy and Department of Biochemistry and Molecular Biology, and [2]Institute of Neuroscience and Department of Psychiatry and Forensic Medicine, School of Medicine, Universitat Autònoma de Barcelona, 08193 Bellaterra, Barcelona, Spain.
[3]Institut de Génétique Moléculaire de Montpellier, Université de Montpellier 1 & 2, 34293 Montpellier, France.
[4]Institut Català de Recerca i Estudis Avançats, 08193 Barcelona, Spain.
*These two authors contributed equally to this work.

disease (Eng *et al.*, 2001; Wilcox *et al.*, 2004), Pompe disease (Thurberg *et al.*, 2006), MPS I (Kakkis *et al.*, 2001), MPS II (Muenzer, 2011), and MPS VI (Harmatz *et al.*, 2006). For MPS VII, data from animal models (O'Connor *et al.*, 1998; LeBowitz *et al.*, 2004) have supported the approval of a phase 1/2 clinical trial (NCT01856218). However, this approach is limited by the permeability of the blood–brain barrier (BBB). As many LSD, including MPS VII, affect the central nervous system (CNS), a strategy that can cross the BBB is necessary.

One approach to address long-term CNS therapy is gene transfer via viral vectors that confer stable and long-term correction. This could provide sustained therapy if a sufficient level of enzyme was secreted in the brain. We and others have demonstrated the potential of different vectors in correcting neuronal pathologies in MPS II (Cardone *et al.*, 2006), MPS IIIA and B (Cressant *et al.*, 2004; Langford-Smith *et al.*, 2012), and MPS VII mice (Bosch *et al.*, 2000a,b; Liu *et al.*, 2007) as well as in larger animal models for the disease (Ciron *et al.*, 2006; Ellinwood *et al.*, 2011). However, clinically relevant gene therapy using common human pathogens as vectors may be complicated by the high incidence of preexisting humoral and cellular immunity (Chirmule *et al.*, 1999; Perreau *et al.*, 2007a).

Human adenoviral vectors induce both innate and adaptive immune responses that trigger the elimination of transgene expression in a relatively short term. Helper-dependent (HD) adenovirus can circumvent the immune response once reaching the nucleus, although they could have been previously neutralized by antiadenovirus antibodies (reviewed by Lowenstein *et al.*, 2007). Canine adenovirus type 2 (CAdV2, or commonly referred to as CAV-2) vectors preferentially transduce neurons, and retrograde axonal transport is efficient, leading to expression of the transgene in many areas of the brain after a single injection (Soudais *et al.*, 2001; Salinas *et al.*, 2009). Compared with human adenovirus serotype 5 vectors, CAV-2 vectors induce a low level of innate response and do not activate the human complement pathways (Keriel *et al.*, 2006; Perreau *et al.*, 2007b). In addition, limited presence and titers of neutralizing antibodies against CAV-2 are found in the human population (Kremer *et al.*, 2000; Perreau and Kremer, 2005). In addition, HD-CAV-2 vectors lead to long-term transgene expression in rodents (Soudais *et al.*, 2004), and have a cloning capacity of $\sim$30 kb. This is an advantage compared with adeno-associated viral (AAV) vectors, as it allows the possibility of modulating therapeutic genes with large, endogenous, or inducible promoters and/or regulatory sequences.

The aim of this study was to test the therapeutic efficacy of intrastriatal injection of an HD-CAV-2 vector expressing $\beta$gluc (HD-RIGIE) in MPS VII mice. We achieved global, long-term correction in MPS VII mouse brains with bilateral striatal injections of HD-RIGIE. We show recovery of biochemical and neuropathological abnormalities throughout the forebrain and midbrain, which led to significant cognitive improvement.

## Materials and Methods

### Animals

We used a tolerant mouse model for MPS VII (Sly *et al.*, 2001) developed from the original $\beta$gluc-deficient mouse (Levy *et al.*, 1996). Heterozygous ($Gus^{mps/+}$) mice, kindly provided by Dr. William S. Sly (St. Louis University School of Medicine, St. Louis, MO), were bred and mutants were identified at 1 month of age by the absence of $\beta$gluc activity from tail clip homogenates. Animal care and experimental procedures were performed in accordance with 86/609/EEC regarding the care and use of animals for experimental procedures and were approved by the Biosafety and the Ethics Committees of the Universitat Autònoma de Barcelona.

### First-generation CAV-2 vectors

E1-deleted CAVGFP has been previously described (Kremer *et al.*, 2000). Vector particles were produced in canine E1 *trans*-complementing cells (DKZeo), originally derived from the canine kidney cell line DK (ATCC CRL6247) (Kremer *et al.*, 2000). Virus from the supernatant were concentrated by precipitation with ammonium sulfate (Schagen *et al.*, 2000) and pooled with the cellular fraction to maximize recovery. This pool was purified using two CsCl density ultracentrifugation steps and CsCl was removed by size exclusion chromatography using PD-10 columns (GE Healthcare), and the virus was stored in 10% glycerol phosphate-buffered saline. Titers were $1.44\times10^{12}$ physical particles (pp)/ml with a pp to infectious particle (ip) ratio of 4:1.

### Production of HD-RIGIE and HD-GFP vectors

HD-RIGIE expressed the human *GUSB* cDNA and GFP under the control of a Rous sarcoma virus promoter. The RIGIE cassette (RSV-IVS-*GUSB*-IRES-EGFP) was generated using classic molecular biology techniques. The human GUSB cDNA was a gift from William Sly (University of St Louis). *Asc*I/*Not*I-digested pHD-RIGIE or pHD-GFP were transfected into $5\times10^6$ DKZeo cells using 18 $\mu$l of Turbofect (Fermentas, Thermo Scientific) for 10 $\mu$g of linearized DNA/10 cm plate. The cells were infected with 100 pp of helper vector/cell. $GFP^+$ cells were collected by flow cytometry 24 hr post-transfection, re-plated, and lysed by three freeze–thaw cycles 20 hr later. Cells were sorted after transfection until at least $2\times10^6$ of $GFP^+$ cells were isolated. The cleared lysates were then incubated on a fresh monolayer of DKZeo cells using helper vector JB$\Delta$5. Twenty-four hours postinfection, $GFP^+$ cells were sorted by flow cytometry, replated, and lysed by three freeze–thaw cycles 20 hr later. The cleared lysate was used for amplification until $3\times10^7$ $GFP^+$ cells were obtained. At each amplification step, DKZeo cells were coinfected with 100 pp/cell of helper vector. Finally, the last amplification occurred in $\sim8\times10^8$ DKCre cells without adding helper vector. JB$\Delta$5 contains a loxP-flanked packaging domain and an RSV-lacZ expression cassette (Soudais *et al.*, 2001, 2004). When propagated in DKCre cells, an $\sim$900 bp fragment containing the packaging domain and part of the RSV promoter was excised (floxed), and the resulting 32.3 kb vector was rendered packaging deficient (Soudais *et al.*, 2004). The helper vector retained a minimal part of the RSV promoter, which promoted *lacZ* expression. To test the level of helper contamination in HD vector preparations, $\beta$-galactosidase activity was assayed by X-gal staining. HD-RIGIE was purified by triple banding on CsCl density gradients: an initial step gradient of 1.25 and 1.45 g/ml, and then two self-forming isopycnic gradients using 1.32 g/ml CsCl as previously described (Soudais *et al.*, 2004). The purified stock was stored at $-80$°C in phosphate-buffered saline (PBS)/10% glycerol.

Physical particles titers were determined by OD at 260 nm and quantitative polymerase chain reaction (qPCR) and were found to be $\sim 1.3 \times 10^{12}$ pp/ml. HD-RIGIE ip were determined by GFP expression. Combined, the pp/ip ratio was 60:1. Because of the relatively low level of GFP from the combination of the weak RSV promoter and IRES in DK cells, this ratio likely overestimates the pp-to-ip ratio. As assayed by X-gal staining and qPCR, helper vector contamination varied between preparations from <1% to ~10%.

### *Animal studies*

Intracranial injections. Mice were anesthetized by intraperitoneal injection of ketamine (10 mg/kg of body weight; Imalgene 500; Rhône-Merieux) and xylazine (1 mg/kg of body weight; Rompun; Bayer) and mounted onto a stereotactic frame (David Kopf Instruments). The skull was exposed by a small incision. A small burr hole was made 1 mm caudal and 1.5 mm lateral to bregma. Three microliters of the vector preparation was loaded into a Hamilton syringe mounted to the stereotactic frame. The tip of the needle was inserted into the striatum 3.0 mm in depth from the skull surface in heterozygous mice and 2.6 mm in mutant mice, and 2 $\mu$l of HD-RIGIE, corresponding to $2 \times 10^9$ pp, was delivered with an ultramicropump (World Precision Instruments) at a rate of 0.5 $\mu$l/min. The needle was slowly withdrawn after an additional 5 min. Mock-injected control animals were injected in the same coordinates with 2 $\mu$l of PBS.

Transient immunosuppression. Cyclophosphamide (CFA; Sigma) was diluted in PBS and administered intraperitoneally at 50 mg/kg of body weight every 2 days, from day −3 to day + 13, considering day 0 as the intracranial injection time, as a modification of the treatment defined by Cao *et al.* (2011).

### *Behavioral tests*

A standardized set of experimental procedures (abbreviated SHIRPA, Giménez-Holt *et al.*, 2002) were used to characterize the phenotype of treated mice. Observation of undisturbed behavior in the home-cage was followed by assessment of fluorimeter tasks.

Rod tests. Motor coordination and equilibrium were assessed by the distance covered and the latency to fall off a horizontal wood rod (1.3 cm diameter) and a wire rod (1 cm diameter) on two consecutive 20 sec trials.

Hanger test. Prehensility and motor coordination were measured as the distance covered on the *wire hang test*, where the animals were allowed to cling (2 mm diameter, 40 cm long) with their forepaws for two trials of 5 sec and a third 60 sec trial. Muscle strength was measured as the time until falling off the wire in the 60 sec trial. All the apparatus were suspended 40 cm above a padded table.

Tertiary screen was designed tailored to neuropsychiatric-like deficits, assessing spontaneous exploratory behavior, anxiety-like behaviors, and cognition in a series of tests involving different degrees of complexity.

Corner test. Neophobia was recorded in a new home-cage by the horizontal (*n* of visited corners) and vertical (*n* and latency of rearings) activity during a period of 30 sec.

Open-field test. Exploratory activity and anxiety-like behaviors were evaluated for 5 min by means of horizontal (crossings of 5 × 5 cm) and vertical (rearings) locomotor activities recorded for each minute of the test.

T-maze. The spontaneous exploratory behavior was tested in a T-shaped maze (arms, length 25 cm). Animals were placed inside the vertical arm of the maze facing the end wall. The performance was evaluated by determining the time elapsed until the animal crossed (four-paw criteria) the intersection of the three arms.

Spatial learning and memory in a 2-day water maze. On day 1, animals were trained to criterion (90% escaping under 60 sec) in a series of cued visible platform trials (7 cm diameter, 1 cm above the water surface, position indicated by a visible 5 × 8 cm striped flag, 20 min intertrial time) in a pool (Intex Recreation; 91 cm diameter, 40 cm deep, 25°C opaque water). This required four platform trials (CUE1–CUE4). The last visible platform trial of any animal was considered to be its posthabituation baseline and was designated CUE4 (cued visible platform trial 4). Mice that failed to find the platform within 90 sec were manually guided to the platform and placed on it for 5–10 sec, the same period as successful animals. Twenty-four hours after the last cued platform trial, animals were tested in a series of four hidden platform trials (PT1–PT4, 20 min apart). In these place-learning tasks, the hidden platform (1.5 cm below the water surface) was located in a new position, opposite the one used for cue learning. Escape latencies were measured with a stopwatch.

### *Biochemical assays*

Detection of lysosomal enzyme activities in tissue extracts. Deeply anesthetized animals were euthanized. The cerebrum was removed and sliced into 2-mm-thick slices using a mouse brain slicer (Zivic Instruments) and stored at −80°C. Tissues were homogenized in lysis buffer (25 m*M* Tris, 75 m*M* NaCl [pH 7.5]; both from Sigma) and centrifuged at 12,000 × *g* for 10 min at 4°C. Ten micrograms of each slice was assayed in a fluorimeter Wallac 1420 Victor3 (Perkin Elmer) for $\beta$gluc or $\beta$-hexosaminidase activity using 10 m*M* 4-methylumbelliferyl-$\beta$-D-glucuronide (Sigma) or 0.01 m*M* 4-methylumbelliferyl-N-acetyl-$\beta$-D-glucosaminide (Sigma) as substrate, respectively.

Detection of $\beta$gluc activity in tissue sections. Animals were anesthetized and perfused with 4% paraformaldehyde, and brains were removed and postfixed. After cryoprotection with 30% sucrose, tissues were embedded in O.C.T. Tissue Tek compound (Miles Scientific) and cut into 10-$\mu$m-thick sagittal or coronal sections. Sections were incubated for 4 hr at 37°C with 0.004% hexazotized pararosaniline in 0.25 m*M* naphtol-AS-BI-$\beta$-D-glucuronide (Sigma).

For volumetric estimation of $\beta$gluc extension, 100-$\mu$m-thick coronal sections were cut at 4°C after 5 hr postfixation with 4% paraformaldehyde using a vibratome (Leica). The whole cerebrum was sectioned, and one in every five sections was stained for $\beta$gluc activity. Transduction volume was estimated based on the number of slides positive for $\beta$-gluc.

GAG quantification. Twenty milligrams of each 2-mm-thick slice was homogenized in papain extraction reagent at 65°C for 3 hr. GAG content was determined using the Blyscan Sulfated Glycosaminoglycan Assay (Biocolor).

### *Histology and immunological assays*

Ten-micrometer-thick cryosections were obtained as described above. Sections were blocked with 2% bovine serum albumin and incubated with rabbit anti-Iba1 (1:500; Wako Chemicals GmbH) or NeuN (1:200; Chemicon, Millipore) overnight at 4°C. Goat antirabbit Alexa Fluor 568 as a secondary antibody (1:200; Molecular Probes) and a Hoechst solution to stain the nuclei (Sigma) were used. To quantify cortical microglia, $Iba1^+$ cells from different sections around the injected area were counted and normalized by the total number of cells counterstained with Hoechst.

Histopathology. About 100-$\mu$m-thick coronal brain sections were postfixed with 4% paraformaldehyde and 1% glutaraldehyde and then with 1% osmium tetroxide, and finally embedded in Epon (all reagents from Sigma). One-micrometer-thick sections were cut and stained with toluidine blue for 30 sec. Histological sections were evaluated morphologically by light microscopy. Sections were further examined, and 200 cells per section and brain structure were counted for each animal to evaluate the percentage of cells without or with very small cytoplasmic vacuoles.

### *Quantitative polymerase chain reaction*

Genomic DNA was obtained from 2-mm-thick brain slices with 0.1 mg/ml of proteinase K (Roche Diagnostics), followed by phenol/chloroform extraction. HD-RIGIE genome copy numbers were measured by qPCR using the Bio-Rad CFX Manager (Bio-Rad Laboratories) and SYBR green PCR (Bio-Rad Laboratories). Briefly, vector sequences and mouse genomic cyclophilin (as reference gene) sequences were simultaneously amplified, and each sample was expressed in terms of its cyclophilin content. The results (vector genome copy number per cell, viral genomes [vg]/cell) were expressed as *n*-fold differences in the transgene sequence copy number relative to the cyclophilin gene copy number (number of vg copies for 2N genome). Samples were considered eligible for the study if the cyclophilin sequence $C_t$ values were $<26$ and were scored vector-negative if the transgene sequence $C_t$ value was $>35$. Thermal cycling conditions comprised an initial denaturing step at 95°C for 3 min, followed by 40 cycles at 95°C for 10 sec, 58°C for 10 sec, and 72°C for 30 sec. Each sample was analyzed in duplicate. Nucleotide sequences of primers are available on request.

### *Statistics*

Values are represented as mean ± SEM. Statistical analyses using Student's *t*-test or one- and two-way ANOVA with *post-hoc* tests were performed for each data set. Repeated-measures ANOVA with a two-factorial design T × G (T = effect of time; G = effect of group) was used for behavioral tests, followed by *post-hoc* Duncan's test. Differences were considered statistically significant if $p < 0.05$.

## Results and Discussion

### *Microglia activation prevents HD-CAV-2 expression in the mouse brain*

CAV-2 can be retrogradely transported to different areas of the brain after a single injection into the striatum (Soudais *et al.*, 2004). Thus, although MPS VII causes global CNS pathology, we asked if a single injection exclusively in the striatum of 8–10-week-old MPS VII mice with $2 \times 10^9$ pp of HD-RIGIE could be of therapeutic efficacy. Animals were euthanized 1 and 6 weeks after the injection. Brains were sectioned into six 2-mm-thick slices, rostral to caudal, as represented in Fig. 1a. GFP expression was observed 1 week postinjection at the injection area and in more distal regions of the brain such as the substantia nigra, containing neurons from the nigrostriatal pathway and projecting their axons to the striatum (Fig. 1b), indicating that CAV-2 vectors maintain retrograde transport in MPS VII brains. Animals euthanized at 1 week posttreatment showed the presence of viral DNA in four of the six slices in the injected hemisphere, with a maximum of $16.83 \pm 4.41$ vg/cell in S2, corresponding to the injection area. We also observed the presence of viral DNA in the contralateral hemisphere although at lower levels, which may be caused by retrogradely transported virus or to leakage of the vector in the cerebrospinal fluid that may lead to the infection of cells in the choroid plexus or in the ependyma around the ventricles, mainly contained in S2 (Supplementary Fig. S1; Supplementary Data are available online at www.liebertpub.com/hum). No DNA was detected in S5 and S6, slices containing the cerebellum and brainstem. However, no GFP expression was observed in the animals euthanized 5 weeks later, neither $\beta$gluc activity (data not shown), correlating with the disappearance of vg in these slices (Fig. 1c).

Delivery of Ad vectors into the CNS induces dose-dependent innate immune responses in the form of acute inflammation, including microglial activation, macrophage recruitment, and T-cell infiltration (Thomas *et al.*, 2001). Consequently, we detected Iba1-positive cells, a marker of microglia, in the brains of animals injected with CAV-2 vector and euthanized 1 week later, correlating with the presence of CAV-2 vg and GFP expression, as seen at the injection area (Fig. 1d) and at the substantia nigra (not shown). Quantification of this signal showed stronger Iba1 staining with first-generation CAV-2 vector than with HD vector at both times analyzed, consistent with a reduction in the immune reaction elicited by HD adenovirus (Fig. 1e). In animals euthanized 6 weeks after injection of HD-RIGIE, mild activation was present only at the injection point, nonstatistically different from brains injected with PBS or noninjected (Fig. 1e). Thus, in contrast to results seen in rats and other mouse strains (Soudais *et al.*, 2004; Sotak *et al.*, 2005), in our hands, E1-deleted and HD-CAV-2 vectors led to short-term transgene expression associated with Iba1 expression. Although HD-Ad vectors do not express viral antigens, innate inflammatory responses to high doses of Ad could trigger elimination of transduced cells even using HD vectors (Muhammad *et al.*, 2012). Moreover, acute toxicity provoked by viral capsid proteins or residual helper vector could also elicit an immune response that could eliminate the transduced cells. Furthermore, in addition to viral proteins, immune responses may have occurred against GFP,

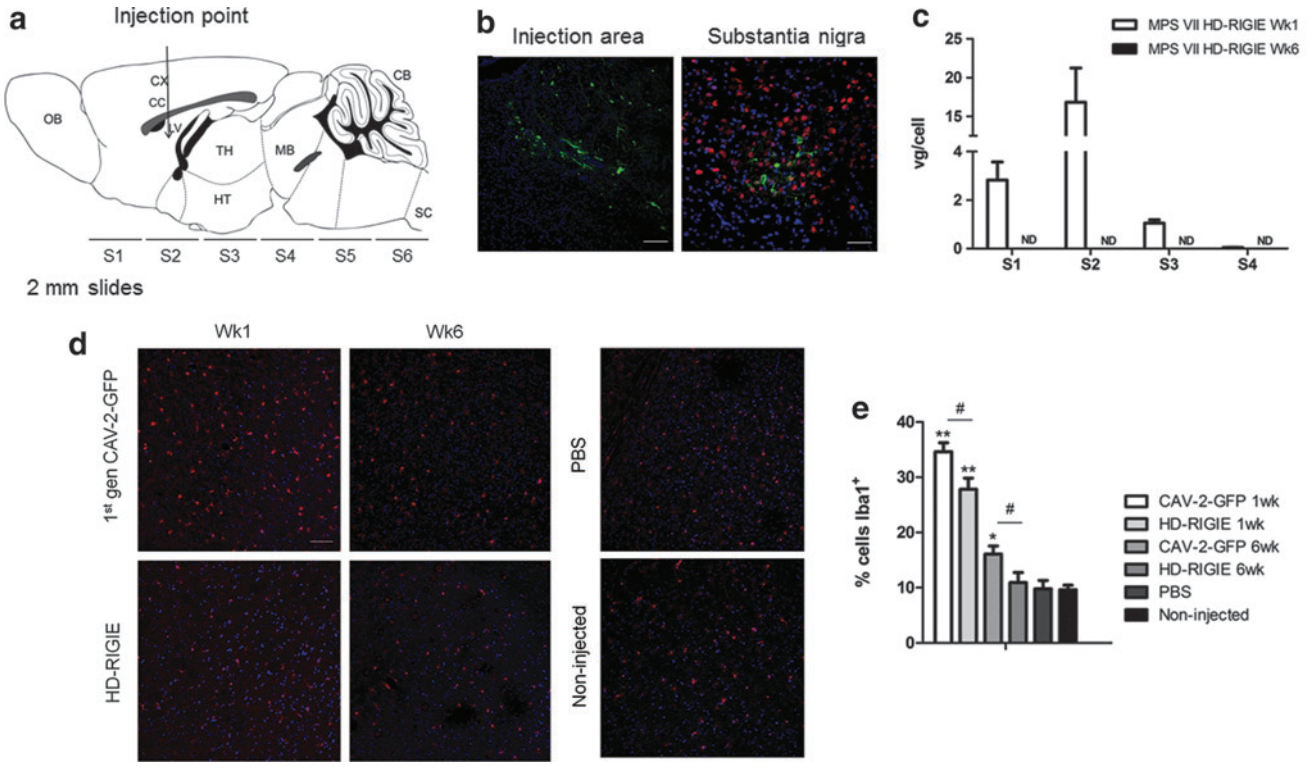


**FIG. 1.** Immune response avoids long-term expression of HD-CAV-2 vectors in CNS **(a)** Mouse brain diagram showing the coordinates used for the administration of HD-RIGIE, and the 2-mm-thick slices analyzed (S1–S6). CB, cerebellum; CC, corpus callosum; CX, cerebral cortex; HT, hypothalamus; LV, lateral ventricle; MB, midbrain; OB, olfactory bulb; SC, spinal cord; TH, thalamus. **(b)** Representative pictures of MPS VII mice injected with HD-RIGIE 1 week earlier: on the left image GFP expression at the injection point (scale bar = 100 $\mu$m), and at the substantia nigra on the right image (scale bar = 50 $\mu$m). Nuclei counterstaining was with Hoechst (blue) and neurons with NeuN (red). **(c)** Viral genomes per cell were quantified by qPCR in 2-mm-thick slices of brains injected with HD-RIGIE 1 and 6 weeks later. Disappearance of viral genomes at 6 weeks was observed (ND, not detected). **(d)** Microglia activation is identified by Iba1 staining (red) at the injection area 1 and 6 weeks after administration (left panel) of CAVGFP (up) and HD-RIGIE (down). Nuclei were counterstained with Hoechst (blue). The right panel shows Iba1 staining in animals injected with PBS or noninjected, as a control. Scale bar = 100 $\mu$m. **(e)** Percentage of Iba1$^+$ cells/field in the different animals injected. Data are mean ± SEM, $n = 2$ animals euthanized at Wk1 and $n = 5$ animals euthanized at Wk6 postinjection; $^*p < 0.05$, $^{**}p < 0.01$ comparing noninjected with vector-injected animals; $^{\#}p < 0.05$ comparing CAVGFP and HD-RIGIE at the same time points. CAV-2, canine adenovirus type 2 vectors; CNS, central nervous system; HD-RIGIE, helper-dependent CAV-2 vector expressing $\beta$-glucuronidase; PBS, phosphate-buffered saline; qPCR, quantitative polymerase chain reaction; Wk, week.

used in this proof-of-principle study as a marker to identify transduced cells. Clearly, a clinical-grade vector would not have a GFP expression cassette.

Because GAG and ganglioside accumulation are associated with chronic CNS inflammation, and the response to viral vector varies between genus, species, and even strains, we transiently immunosuppressed the animals with 50 mg/kg CFA (Supplementary Fig. S2), previously used to reduce inflammation and neutralizing antibody formation (Cao *et al.*, 2011). Iba1 immunohistochemistry in the HD-RIGIE-injected and transiently immunosuppressed mice showed no activation compared with control mice (Fig. 2a). More importantly, $\beta$gluc activity was detected in brain slices from MPS VII mice injected with HD-RIGIE 6 weeks earlier (Fig. 2b). Thus, 50 mg/kg of CFA treatment was followed for the rest of the experiments. CFA is widely used to treat autoimmune diseases, to prevent rejection after allograft organ transplantation and to suppress antibody formation (Moore *et al.*, 2006). Probably other transitory immunosuppressants such as cyclosporine A could have also worked in our model. However, the clinical relevance of this treatable inflammatory response in mice is unknown because mice and humans have notably different reactions in many cases (Seok *et al.*, 2013).

### *Lysosomal enzyme activities in HD-RIGIE-injected MPS VII mice*

On the basis of these results, a group of 8–10-week-old animals was injected bilaterally in the striata (Fig. 1a). Control littermates (heterozygous and mutant mice) were mock injected with the same volume of PBS and treated with CFA at the same time and dose. Mice were euthanized at 6 and 16 weeks, and $\beta$gluc activity was assayed using *in situ* coloration by incubating slices with hexazotized pararosaniline in 0.25 m*M* naphtol-AS-BI-$\beta$-D-glucuronide in 100-$\mu$m-thick sections, one in every 5 sections, along the whole brain. This is an insensitive assay that stains $\beta$gluc activity in red. $\beta$gluc activity was not detected in PBS-treated or heterozygous mice, showing the low sensitivity of

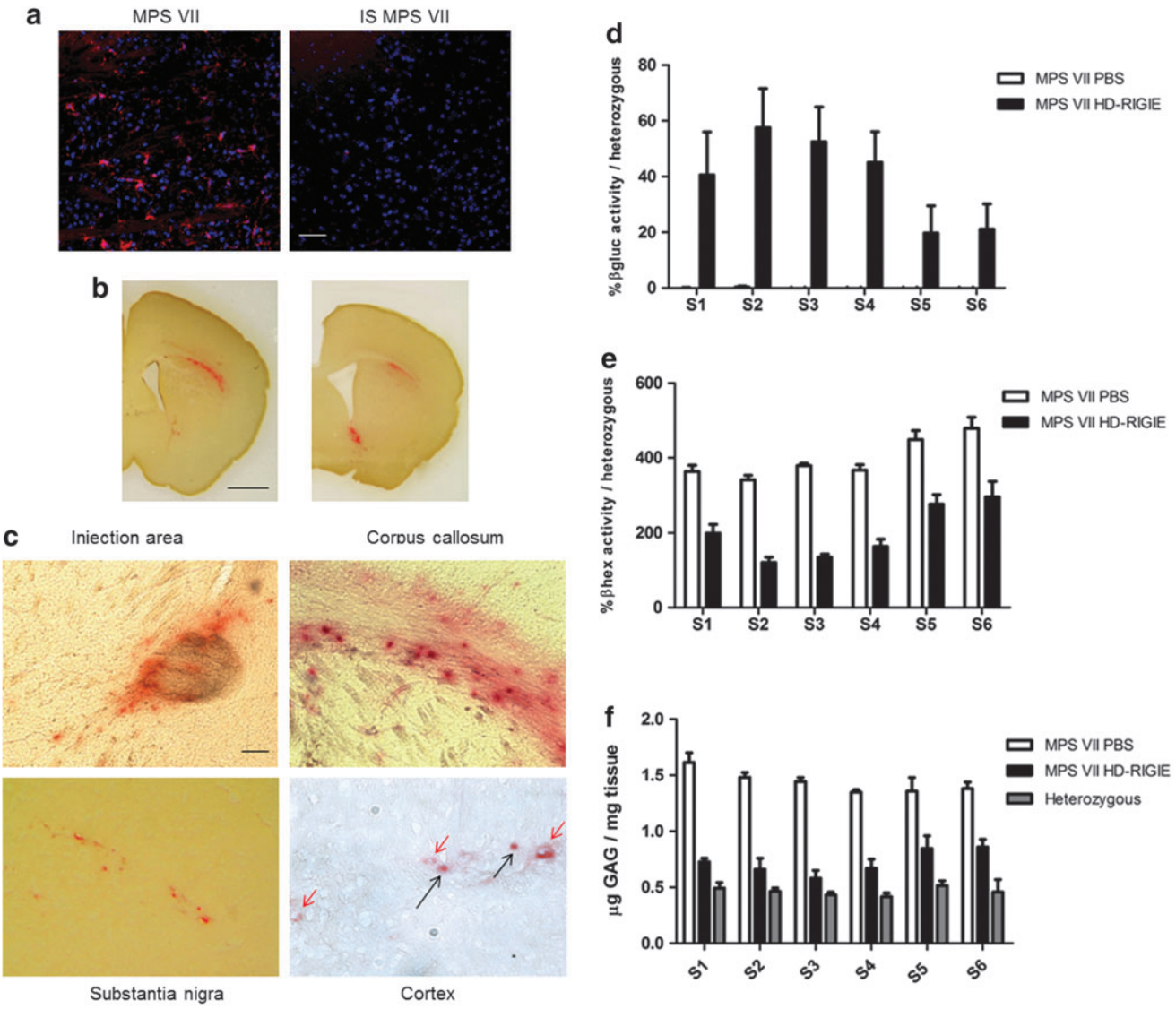


**FIG. 2.** Lysosomal enzyme activity and GAG accumulation analysis 6 weeks postinjection. **(a)** Iba1 staining (red) in immunocompetent (left image) or transiently immunosuppressed MPS VII mice with 50 mg/kg of cyclophosphamide (right image) show lack of activated microglia after HD-RIGIE administration (scale bar = 50 $\mu$m; nuclei were counterstained with Hoechst [blue]). $\beta$gluc activity (red) in **(b)** 100-$\mu$m-thick (scale bar = 1 mm) and **(c)** 10-$\mu$m-thick brain slices at the injection area and other distal areas such as corpus callosum, substantia nigra, and cortex; red and black arrows indicate endothelial cells and cortical neurons, respectively, identified by morphology in cortex cryosections (scale bar = 100 $\mu$m). $\beta$gluc activity **(d)**, secondary elevation of lysosomal enzyme $\beta$-hexosaminidase **(e)**, and GAG accumulation **(f)** in 2-mm-thick slice homogenates from MPS VII mice injected with PBS or HD-RIGIE and compared with $\beta$gluc activity in heterozygous mice ($p < 0.01$ for $\beta$gluc; $p < 0.01$ in S5 and S6 for $\beta$hex; $p < 0.01$ in S5 and S6 for GAG). No statistically significant differences were seen among heterozygous and HD-RIGIE-treated mice in slices spanning between S1 and S4. Data are mean ± SEM; $n = 7$ for each experimental group.

the assay. In HD-RIGIE-treated MPS VII mice, we detected $\beta$gluc activity in striatum, several areas of the cortex, corpus callosum, substantia nigra, and around ventricles (Fig. 2b and c), consistent with the efficient retrograde transport described for CAV-2 vectors (Soudais *et al.*, 2001; Salinas *et al.*, 2009). The majority of transduced cells had morphology suggesting that they were neurons. We also detected cells underlying blood vessels, consistent with endothelial cell morphology (Fig. 2c). Overall, based on this assay, we estimated a transduction area with a diameter of 4 mm around the injection area.

The brain of some of these animals ($n = 7$ for each group) was sliced into 2-mm-thick sections, as described in Fig. 1a, and protein extracts were prepared. For each slice, we measured $\beta$gluc and $\beta$-hexosaminidase ($\beta$hex) activity using a more sensitive fluorimetric assay. In several MPS diseases, $\beta$hex activity is elevated when another lysosomal enzyme activity is missing, likely because of transcription factor EB (TFEB) (Sardiello *et al.*, 2009). Data were plotted as the percentage of activity of each enzyme compared with heterozygous mouse levels, which have a normal phenotype (Fig. 2d and e). This MPS VII mouse model was created to

be tolerant for human βgluc, by expressing a mutant inactive form of human βgluc, although protein levels are almost undetectable in most tissues (Sly *et al.*, 2001). Notably, βgluc activity in heterozygous mice is 80% of the wild-type animals (data not shown). As seen in Fig. 2d, no βgluc activity was detected in mock-treated MPS VII mice. By contrast, HD-RIGIE-treated mice showed near 50% of the βgluc activity found in heterozygous animals from slice 1 to 4, with the maximum at the injection area (S2) (up to 57.55% ± 14.02%) and around 20% in S5 and S6, corresponding to cerebellum and brainstem ($p < 0.01$). Equally relevant, we found a significant decrease in the secondary elevation of βhex in all brain areas, consistent with the biochemical correction of βgluc deficiency (Fig. 2e). βhex activity reached heterozygous levels (120.79% ± 14.015% and 120.228% ± 12.857% of heterozygous mice) in S2 and S3, respectively. We found an inverse correlation between βgluc and βhex activities in all sections. Notably, there was not a significant difference between HD-RIGIE-treated and heterozygous mice for slices S1–S4. Therefore, by administering HD-RIGIE into the striatum, we could detect CAV-2 vg and transgene activity throughout the cerebrum, which led to global protein transfer in the brain.

In MPS VII mice euthanized 16 weeks post-HD-RIGIE injection, we also found βgluc activity ($n = 4$ for each group) in tissue sections of brains for a total of 4 mm (Fig. 3a). Similar to animals analyzed 6 weeks post-HD-RIGIE injection, enzyme activity detected by fluorimetry in protein homogenates of 2-mm-thick slices showed a high level of transduction, with βgluc activity found in all the slices, spanning the whole brain. HD-RIGIE-injected mice expressed 40–65% of heterozygous activity from slices S1 to S4. The maximum activity was observed near the injection point in S2 and S3, with 63.8% ± 2.75% and 60.86% ± 4.88% of the activity of heterozygous animals, respectively (Fig. 3b). Activities around 20% were also detected in the slices corresponding to cerebellum and brainstem (S5 and S6), and no enzyme activity was detected in the MPS VII animals injected with PBS (Fig. 3b).

βhex activity showed similar pattern as in animals analyzed at 6 weeks postinjection and inversely correlated to the amount of βgluc observed in each slice. While MPS VII mice treated with PBS had around 400% of heterozygous activity, HD-RIGIE-injected MPS VII mice showed correction in S1, S5, and S6, and were not significantly different from heterozygous mice in S2, S3, and S4 (Fig. 3c).

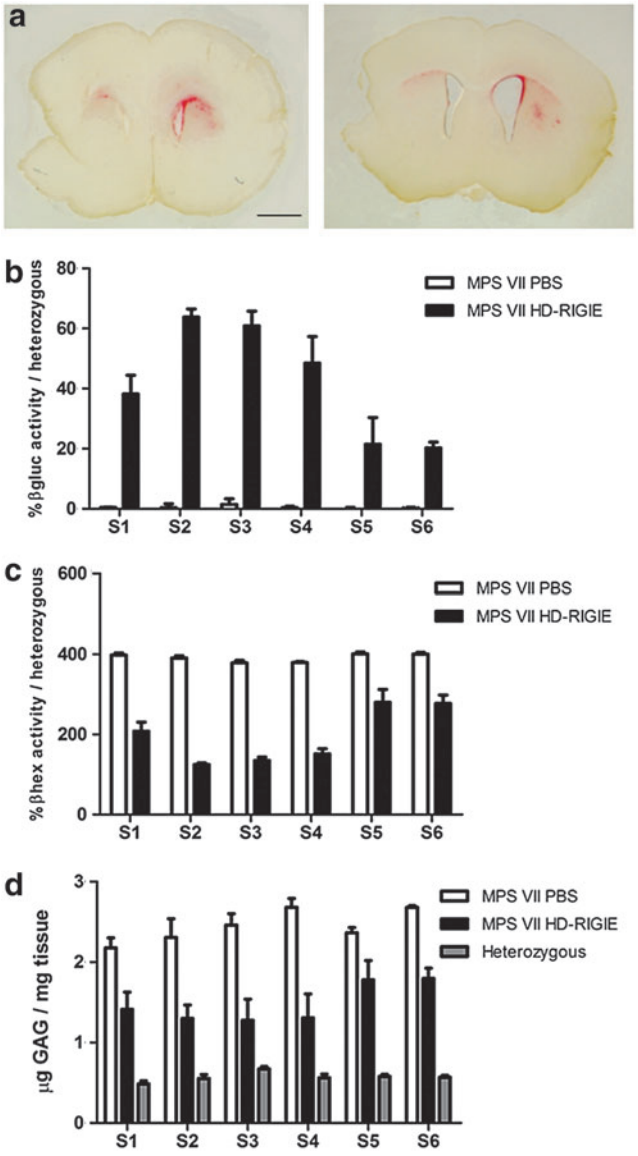


**FIG. 3.** Lysosomal enzyme activity and GAG accumulation analysis 16 weeks after the treatment. βgluc activity in **(a)** 100-μm-thick slices (red; scale bar = 1 mm) and **(b)** 2-mm-thick slice homogenates, **(c)** secondary elevation of β-hexosaminidase activity, and **(d)** GAG accumulation in 2-mm-thick slice homogenate slices in MPS VII mice injected with PBS or HD-RIGIE compared with heterozygous mice ($p < 0.01$ for βgluc; $p < 0.01$ in S1, S5, and S6 for βhex; and $p < 0.01$ for GAG). Data are mean ± SEM; $n = 4$ for each experimental group.

### *GAG accumulation in MPS VII-treated mouse brain extracts*

MPS VII is characterized by the inability to degrade glucuronic acid-containing GAG. GAG quantification was used to evaluate the therapeutic effect of the HD-RIGIE treatment at 6 and 16 weeks post-HD-RIGIE injection. We reduced GAG accumulation in all sections of the brain, consistent with increased βgluc and reduced βhex activities observed in Figs. 2 and 3. Mice were treated around 8–10 weeks of age and were analyzed 6 or 16 weeks later, that is, when they reached 3.5 or nearly 6 months of age. In the first experimental group, MPS VII animals had GAG levels near 1.5 μg/mg of tissue in all the slices of the brain, threefold more than heterozygous mice. Animals injected with HD-RIGIE showed no statistically significant differences in GAG levels between S1 and S4 compared with heterozygous mice and a 40% reduction in S5 and S6 compared with the same slices of MPS VII-PBS mice ($p < 0.01$) (Fig. 2f).

MPS VII mice analyzed at 6 months showed greater GAG accumulation in all the slices, with levels reaching values of 2.7 μg/mg of tissue, fivefold higher than heterozygous mice. GAG quantification in MPS VII-HD-RIGIE mice showed a 50% decrease in S2, S3, and S4 and between 30% and 40% in S1, S5, and S6 compared with nontreated mutant mice (Fig. 3d). Although there were still statistically significant

differences between HD-RIGIE-treated and heterozygous animals in S2 and S3 slices ($p < 0.01$), this reduction was greater at 6 months of age, when the pathology of the disease was much more severe and these animals were at the end of their life expectancy.

### *Correction of pathology in the HD-RIGIE-injected mouse brain*

We evaluated brain pathology in treated animals 6 and 16 weeks postinjection in semi-thin sections from the cortex, striatum, and meninges around injection point (S2), cortex and striatum at S3 and S4 levels, and hippocampus.

Representative images of the different brain regions from animals euthanized 6 weeks postinjection showed a significant correction of neurons, and glial cells, which presented with greater distended lysosomal morphology in all areas analyzed (Fig. 4). More than 90% of the cells in the injection area and between 83% and 89% in more distal regions showed no, few, or minuscule vacuoles, compared with large vacuoles in nontreated MPS VII animals (Table 1). An additional group of animals received HD-RIGIE only in one hemisphere. Six weeks after treatment, contralateral hemispheres showed also correction in S2, mainly in striatum and cortex (Supplementary Fig. S3). Therefore, even when injecting in a single hemisphere, there was evidence of vg and lysosomal correction in the contralateral hemisphere (Supplementary Figs. S1 and S3). Although we cannot discard transport in the CSF and transduction of perivascular cells in this hemisphere via HD-RIGIE leakage from the injected area, the most plausible explanation would be via axonal transport of the vector and/or $\beta$gluc.

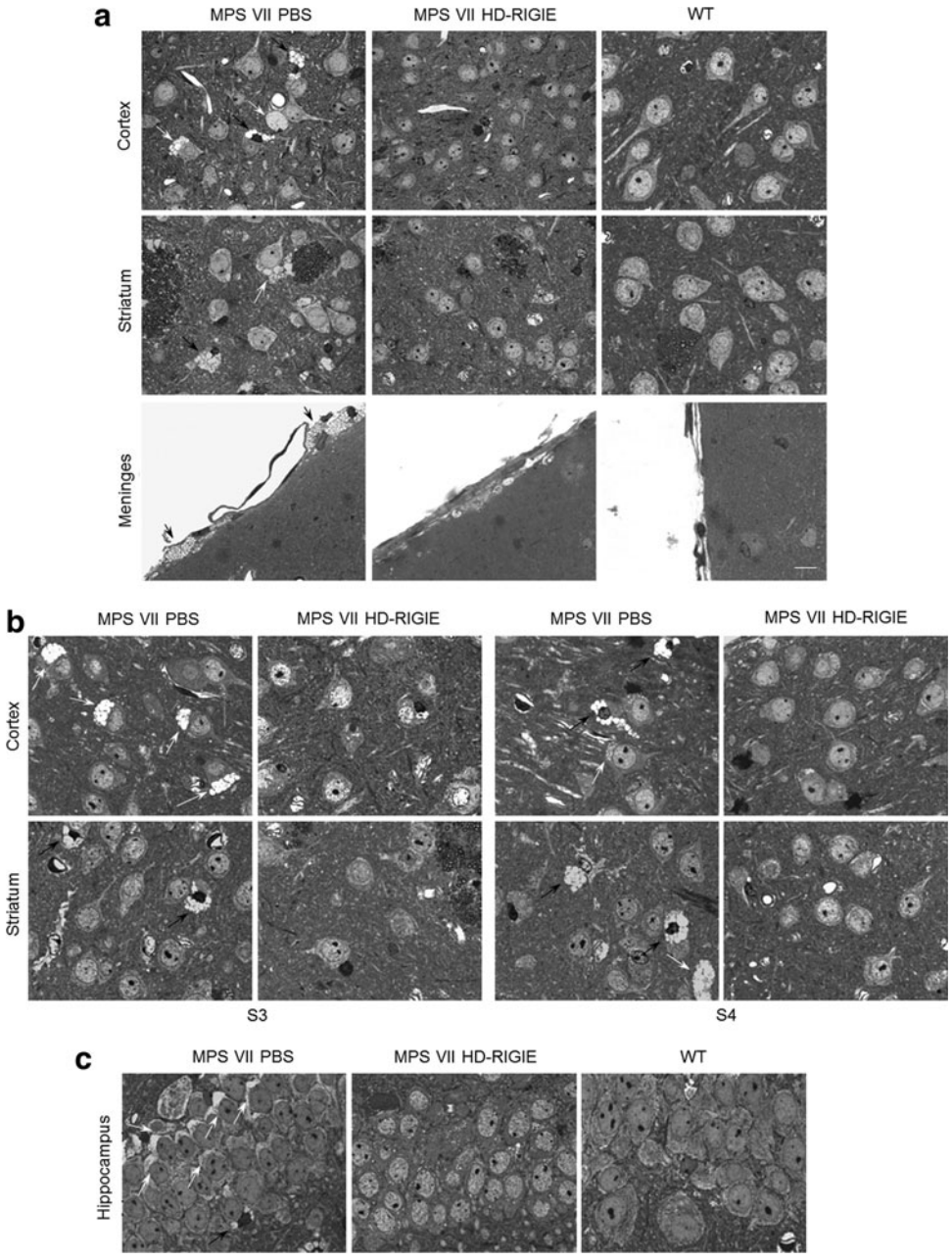


**FIG. 4.** Histopathological studies 6 weeks postinjection. Semi-thin sections of different brain areas surrounding the injection point were stained with toluidine blue to highlight the enlargement of vacuoles containing lysosomal storage material as seen in PBS-treated MPS VII mice. Representative images from **(a)** cortex, striatum, and meninges in MPS VII PBS (left), MPS VII HD-RIGIE (middle), and WT mice (right) at injection area, and at more distal areas **(b)**, slices in S3 (left panel) and S4 (right panel), and **(c)** hippocampus. HD-RIGIE-treated mice show a pattern similar to WT animals in all tissues analyzed. Quantification of corrected cells is described in Table 1. Scale bar = 20 $\mu$m. Black and white arrows indicate vesicle accumulation in glial cells and neurons, respectively.

TABLE 1. PERCENTAGE OF CORRECTED CELLS PRESENT IN CENTRAL NERVOUS SYSTEM STRUCTURES QUANTIFIED IN HISTOPATHOLOGICAL IMAGES FROM ANIMALS TREATED WITH HD-RIGIE AND ANALYZED AFTER 6 OR 16 WEEKS

| | *Injection area* | | *Distal regions* | | | | |
|---|---|---|---|---|---|---|---|
| | *Cortex (%)* | *Striatum (%)* | *Cortex (S3) (%)* | *Striatum (S3) (%)* | *Cortex (S4) (%)* | *Striatum (S4) (%)* | *Hippocampus (%)* |
| HD-RIGIE 6wk | 90 ± 5 | 95 ± 3 | 86 ± 5 | 89 ± 4 | 83 ± 9 | 85 ± 10 | 88 ± 6 |
| HD-RIGIE 16wk | 94 ± 3 | 96 ± 2 | 90 ± 6 | 91 ± 5 | 88 ± 7 | 90 ± 5 | 85 ± 9 |

HD-RIGIE, helper-dependent CAV-2 vector expressing β-glucuronidase; wk, week.
Data are mean ± SEM. Three fields of each animal and area were counted. S3 and S4 correspond to the slides represented in Fig. 1a.

Consistent with the biochemical correction, histopathology of proximal and distal areas to the injection point showed a significant reduction of enlarged lysosomes in neurons and glial cells in mice euthanized 16 weeks post-HD-RIGIE injection (Fig. 5). We also quantified the percentage of cells with recovered phenotype in animals treated 16 weeks earlier, and we found between 90% and 96% in the injection area and higher than 85% in more distal regions (Table 1).

Together, these data demonstrated that HD-RIGIE therapy led to stable transgene expression at least for 16 weeks

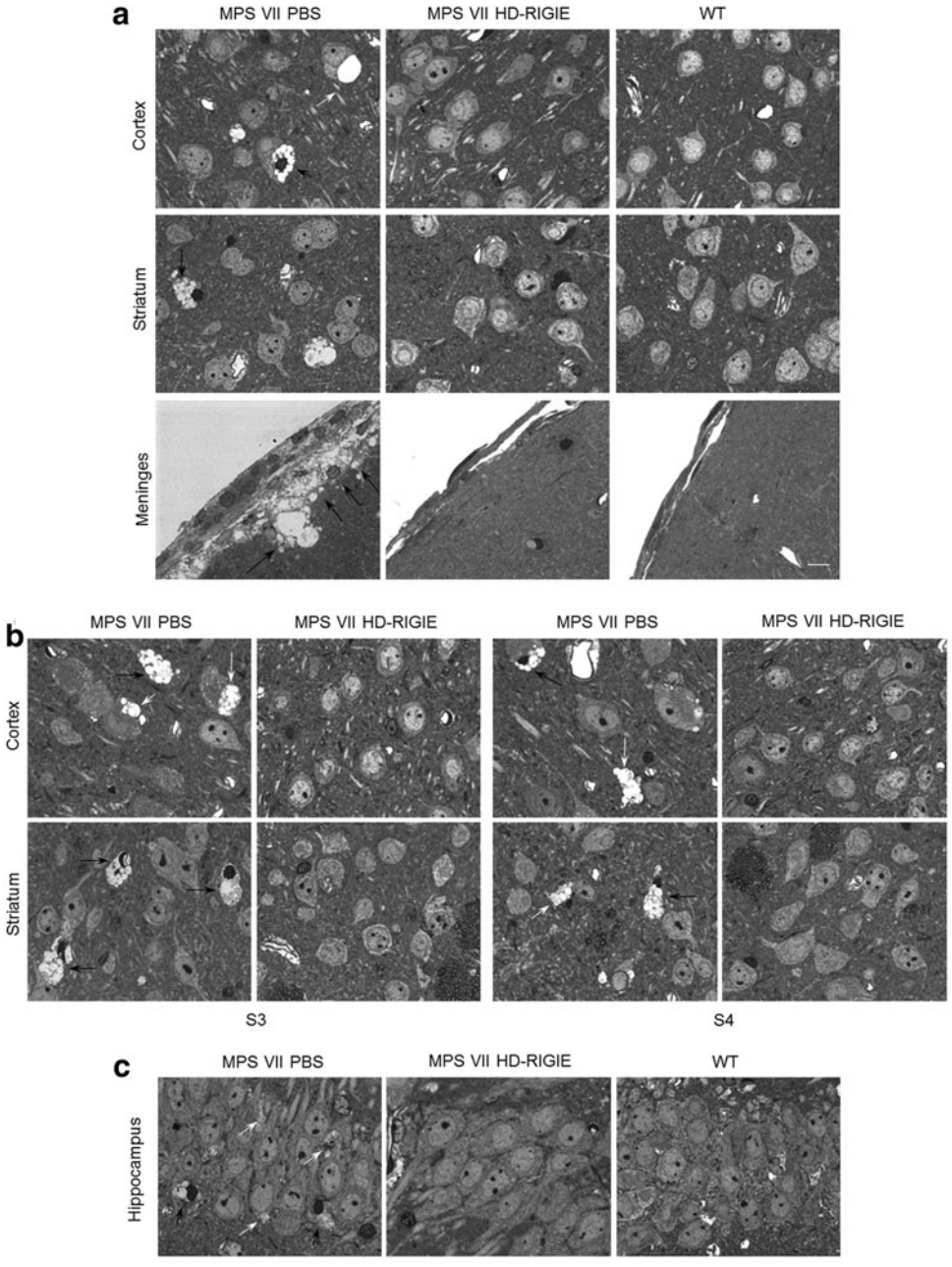


**FIG. 5.** Histopathological studies 16 weeks postinjection. Representative images from **(a)** cortex, striatum, and meninges in MPS VII PBS (left), MPS VII HD-RIGIE (middle), and WT mice (right) at injection area, and at more distal areas **(b)**, slices in S3 (left panel) and S4 (right panel), and **(c)** hippocampus. HD-RIGIE-treated mice show a pattern similar to WT animals in all tissues analyzed. Quantification of corrected cells is described in Table 1. Scale bar = 20 μm. Black and white arrows indicate vesicle accumulation in glial cells and neurons, respectively.

throughout the mid- and the forebrain of MPS VII mice after bilateral striatal injections and that unilateral injection improved MPS VII pathology in the contralateral hemisphere.

### *HD-RIGIE reverses MPS VII-associated cognitive deficits*

In MPS VII mice, progressive impairment in peripheral tissues and in the CNS causes behavioral alterations. Although MPS VII is a multisystem disease, our aim was to test the suitability of HD-CAV-2 in treating a global neurodegenerative disease. We analyzed the behavior of treated mice, mainly using animals treated for 6 weeks, because the poor overall physical condition of 6-month-old animals, at the end of their life, precluded interpretation of the results. This physical impairment may also contribute to the reduction in behavioral performances reported at different ages (Liu *et al.*, 2005; Chen *et al.*, 2012). For that reason, we chose tests with conditions and degree of difficulty to provide convergent validity (Gimenez-Llort *et al.*, 2002, 2007).

We evaluated spontaneous behavior and sensorimotor functions, behavioral and psychological symptoms (locomotor and exploratory activity, anxious-like behaviors), as well as cognition (learning and memory). Impairment of some muscle and lower motor neuron functions was found when MPS VII animals were assessed in the two-rod and hanger tests (Fig. 6a) ($p < 0.001$). MPS VII mice showed the poorest coordination and prehensility and lower muscular strength ($p < 0.05$), whereas equilibrium was normal. HD-RIGIE treatment restored coordination and improved prehensility (both, $p < 0.05$) but did not modify muscular strength. Not surprisingly, this suggests that some functions depending on somatic development will require systemic or a long-term treatment from early developmental stages (O'Connor *et al.*, 1998).

Classical unconditioned tests such as the corner test (Fig. 6b), the T-maze test (Fig. 6c), and open-field test (Fig. 6d–f) involving different levels of anxiogenic conditions indicated reduced horizontal and vertical locomotor activities. Severe problems to interact with the environment were also evident by reduced exploration (Fig. 6d and e) (Time, T, $p < 0.01$; Time × Group, T × G, $p < 0.05$; Group, G, $p < 0.001$). HD-RIGIE treatment reversed the reduced activity in the corner test (Fig. 6b; Corners and Rearings, $p < 0.001$), freezing episodes ($p < 0.001$), forward locomotion ($p < 0.001$), the delay in the onset of vertical exploratory behaviors ($p < 0.05$), and the total vertical activity ($p < 0.001$).

In the T-maze for spontaneous alternation, MPS VII animals showed the poorest performance with a significant delay in the consecution of the behavioral events (Fig. 6c; latency to get started and to reach the intersection, both $p < 0.05$). Only 43% completed the test, while investing more time (exploratory efficiency, $p < 0.01$) and committing more errors ($p < 0.01$). HD-RIGIE treatment increased the incidence to 86%, corrected the delay to reach the intersection ($p < 0.05$), and reduced the number of errors ($p < 0.05$), although it did not modify the exploratory efficiency.

Assessment of spatial learning and memory in the 2-day water maze demonstrated that MPS VII mice had the poorest total cognitive capacity and deficits in the learning acquisition process as well as in both short- and long-term memories. Although all groups showed a similar acquisition curve of the simple cued-learning task (Fig. 6g; T, $p <$ ,0.001), MPS VII mice had the poorest total cognitive capacity ($p < 0.05$) and final outcome, as shown by their baseline performance in the last visible platform trial ($p < 0.05$), which was restored to heterozygous levels by HD-RIGIE treatment.

Place learning (PT) is a more difficult task because the platform is hidden and its location changed. Heterozygous animals spent more time in the platform's prior location, but once it was found, they efficiently remembered it. In contrast, the behavior of MPS VII during the first PT trial (PT1) was similar to their first contact with the maze (CUE1). Moreover, the overall cognitive ability of MPS VII mice to solve the tasks was lower (Fig. 6h; $p < 0.01$), and long- and short-term memory was impaired (Fig. 6i; PT1-CUE4, $p < 0.05$; and Fig. 6i; PT1-PT4, $p < 0.01$, respectively) as compared with heterozygous and MPS VII HD-RIGIE mice (both, $p < 0.05$). HD-RIGIE treatment rescued the cognitive deficits (Fig. 6g–i) and, most importantly, the total learning and memory capacities (Fig. 6h).

Our experimental design shows that reduction in behavioral performances was mostly caused by a reduced exploratory activity, has a strong influence of novelty, and is limited by the cognitive capacity of the animal to confront the situation. Such deficiencies were more clearly shown in the time course of the performances and were improved, and even corrected, by HD-RIGIE treatment. Finally, the cognitive impairment of MPS VII mice was severe, as not only short- and long-term learning and memory processes but also the strategies to solve the tasks and the cognitive capacity, itself, were compromised. Cognitive dysfunction worsened with the difficulty (hidden PT), and their cognitive plasticity did not benefit from previous experience. In contrast, heterozygous animals remembered the prior location of the platform and insisted on searching for it. Place task learning also evidenced impairment in short-term memory and deficits in the total learning capacity of MPS VII as compared with heterozygous mice. However, the major findings are that HD-RIGIE treatment completely rescued the cognitive deficits, mostly in short-term memory, and the total learning and memory capacities.

Notably, this is the first study in which elevated enzyme levels in brain, reduction of lysosomal storage, and reversal of cognitive deficits have been observed after intracranial injection of a HD-CAV-2 vector in a mouse model of disease. Previous experiments with HD adenoviral vectors had demonstrated their potential in the treatment of gliomas after direct tumor injection (Muhammad *et al.*, 2012) and in animal models for different diseases after intravenous injection (Dimmock *et al.*, 2011; Crane *et al.*, 2012). Recently, HD-CAV-2 vector was injected in the CNS of a mouse model of MPS IIIA, but although discrete long-term transgene expression was obtained, only 9% reduction of storage material was achieved at the injection point and no cognitive reversion was described (Lau *et al.*, 2012). One significant difference was the transient immunosuppression in the MPS VII animals to achieve robust, long-term transgene expression in this study. However, immune response is dose dependent. The low transgene expression obtained in MPS IIIA animals may allow the escape of the immune response, but it is not sufficient to elicit a significant therapeutic effect in the MPS IIIA model. Similarly, Dindot *et al.* (2011) achieved long-term expression after intrathecal administration of

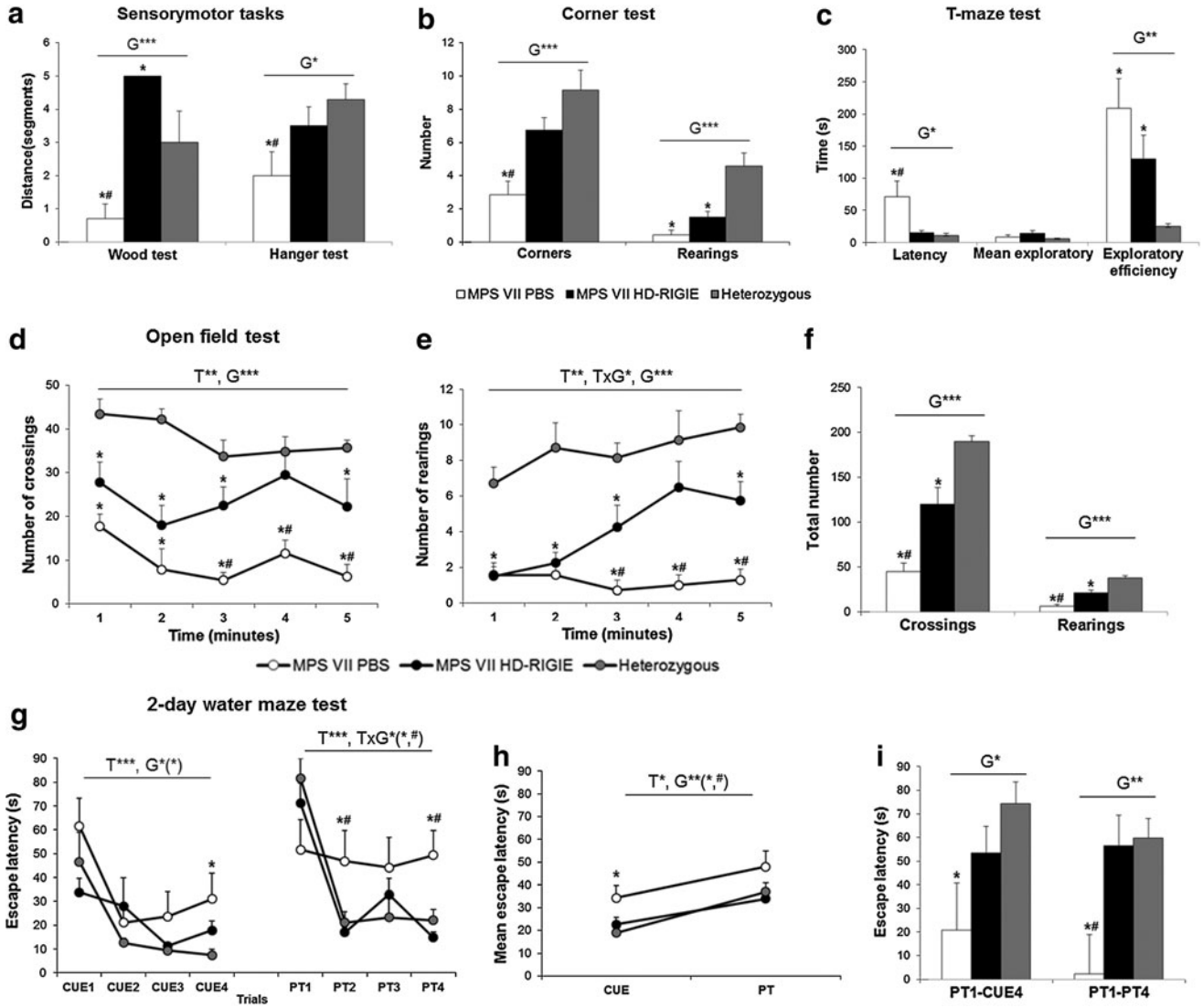


**FIG. 6.** Behavioral effects of HD-RIGIE in MPS VII mice. **(a)** Sensorimotor tasks. HD-RIGIE treatment allowed complete restoration of coordination in the wood test, while prehensility in the hanger test, measured as the latency to fall, was improved by the treatment. **(b)** Corner test. MPS VII mice showed reduction of total horizontal (crossings) and vertical (rearings) activities, which were significantly improved by HD-RIGIE treatment. **(c)** T-maze test. HD-RIGIE treatment completely corrected the increased latency to reach the intersection of the maze and improved the overall capacity to solve the paradigm (exploratory efficiency) but did not modify the mean exploratory time in the arms. **(d–f)** Open-field test. HD-RIGIE corrected the reduction of horizontal and vertical activity exhibited in the open-field test, as shown by the temporal course of the behavior **(d**, crossings 1–5; **e**, rearings 1–5) and the accumulated counts **(f)**. **(g)** Two-day water maze. Acquisition curves. Latency to find the visible (CUE1–CUE4) and hidden (PT1–PT4) platform in a 2-day water maze for mice. Decrease of escape latencies through the cue-learning task was similar between the groups, but MPS VII showed the poorest baseline performance in the last visible platform trial. In the reversal place-learning task, the MPS VII mice showed significantly worse escape latencies as compared with the good acquisition shown by HET and MPS VII-treated mice. **(h)** Long-term memory. Mean escape latency in the cue- and place-learning tasks. All the groups showed significantly higher mean escape latencies when the platform was hidden as compared with the previous task. However, MPS VII mice showed a worse long-term performance as compared with HET and treatment with HD-RIGIE restored this deficit. **(i)** Long-term and short-term memories. Long-term memory deficits observed by means of the differences in the escape latency after the 24 hr interval (PT1–CUE4) were lacking in HD-RIGIE-treated animals. Short-term memory deficits observed in the place-learning task (PT1–PT4) were reversed in HD-RIGIE-treated animals. Data are mean ± SEM; $*p<0.05$, $**p<0.01$, $***p<0.001$ comparing HET with the other two MPS groups; $^{\#}p<0.05$ comparing MPS VII PBS with MPS VII HD-RIGIE. T, time; G, group; T × G, time × group; $n=7$ for each group.

human HD adenovirus coding for GFP in a wild-type mouse. The authors administered $2.5\times10^9$ pp/mouse into the 40 $\mu$l volume that constitutes the mouse CSF. Here we injected a similar amount of pp but concentrated into a single injection in the brain parenchyma that may certainly lead to a higher local immune response as demonstrated by Iba1 immunohistochemistry (Fig. 1).

In summary, we have shown that intrastriatal injection of HD-RIGIE resulted in stable expression of $\beta$gluc in the brains of MPS VII mice, inducing correction in the brain of

these animals. These findings are relevant to the treatment of neurological abnormalities in humans with lysosomal storage diseases and may also be possibly used in neurodegenerative disorders, although it would be necessary to assess the vector performance in large animal models of the disease.

### Acknowledgments

We thank the Vector Production Unit at Center of Animal Biotechnology and Gene Therapy (CBATEG; Universitat Autònoma de Barcelona), which was supported by the Association Française contre les Myopathies, for producing CAVGFP, and Meritxell Puig, David Ramos, and Angel Vázquez (CBATEG) for technical assistance. We are indebted to Laia Acarin (Universitat Autònoma de Barcelona) for help with Iba1 immunohistochemistry. We thank the Montpellier RIO imaging and, in particular, Miriam Boyer-Clavel for help with flow cytometry.

G.P. and B.G.-L. were recipients of predoctoral fellowships (G.P. from the Generalitat de Catalunya [2009FI_B00219] and B.G.-L. from the Ministerio de Educación [EDU/3445/2011]). E.J.K. is an Inserm fellow. Funding was provided by the European Commission through European Community's 7th Framework Program (FP7/2007–2013; Grant 222992, BrainCAV to E.J.K. and A.B.), the Region Languedoc Roussillon (ARPE and CTP 115277 to E.J.K.) and AGAUR (2009 CTP 00030) to M.C., the Fondation de France (Grant #2008005416), Vaincre les Maladies Lysosomales, and the E-RARE 2009 program (project CAV-4-MPS funded by E-RARE to E.J.K. and to A.B. [Instituto de Salud Carlos III-PS0902674]).

### Author Disclosure Statement

No competing financial interests exist.

### References

Birkenmeier, E.H., Davisson, M.T., Beamer, W.G., *et al.* (1989). Murine mucopolysaccharidosis type VII. Characterization of a mouse with beta-glucuronidase deficiency. J. Clin. Invest. 83, 1258–1266.

Bosch, A., Perret, E., Desmaris, N., and Heard, J.M. (2000a). Long-term and significant correction of brain lesions in adult mucopolysaccharidosis type VII mice using recombinant AAV vectors. Mol. Ther. 1, 63–70.

Bosch, A., Perret, E., Desmaris, N., *et al.* (2000b). Reversal of pathology in the entire brain of mucopolysaccharidosis type VII mice after lentivirus-mediated gene transfer. Hum. Gene Ther. 11, 1139–1150.

Cao, H., Yang, T., Li, X.F., *et al.* (2011). Readministration of helper-dependent adenoviral vectors to mouse airway mediated via transient immunosuppression. Gene Ther. 18, 173–181.

Cardone, M., Polito, V.A., Pepe, S., *et al.* (2006). Correction of Hunter syndrome in the MPSII mouse model by AAV2/8-mediated gene delivery. Hum. Mol. Genet. 15, 1225–1236.

Chen, Y.H., Claflin, K., Geoghegan, J.C., and Davidson, B.L. (2012). Sialic acid deposition impairs the utility of AAV9, but not peptide-modified AAVs for brain gene therapy in a mouse model of lysosomal storage disease. Mol. Ther. 20, 1393–1399.

Chirmule, N., Propert, K., Magosin, S., *et al.* (1999). Immune responses to adenovirus and adeno-associated virus in humans. Gene Ther. 6, 1574–1583.

Ciron, C., Desmaris, N., Colle, M.A., *et al.* (2006). Gene therapy of the brain in the dog model of Hurler's syndrome. Ann. Neurol. 60, 204–213.

Crane, B., Luo, X., Demaster, A., *et al.* (2012). Rescue administration of a helper-dependent adenovirus vector with long-term efficacy in dogs with glycogen storage disease type Ia. Gene Ther. 19, 443–452.

Cressant, A., Desmaris, N., Verot, L., *et al.* (2004). Improved behavior and neuropathology in the mouse model of Sanfilippo type IIIB disease after adeno-associated virus-mediated gene transfer in the striatum. J. Neurosci. 24, 10229–10239.

Dimmock, D., Brunetti-Pierri, N., Palmer, D.J., *et al.* (2011). Correction of hyperbilirubinemia in gunn rats using clinically relevant low doses of helper-dependent adenoviral vectors. Hum. Gene Ther. 22, 483–488.

Dindot, S., Piccolo, P., Grove, N., *et al.* (2011). Intrathecal injection of helper-dependent adenoviral vectors results in long-term transgene expression in neuroependymal cells and neurons. Hum. Gene Ther. 22, 745–751.

Ellinwood, N.M., Ausseil, J., Desmaris, N., *et al.* (2011). Safe, efficient, and reproducible gene therapy of the brain in the dog models of Sanfilippo and Hurler syndromes. Mol. Ther. 19, 251–259.

Eng, C.M., Guffon, N., Wilcox, W.R., *et al.* (2001). Safety and efficacy of recombinant human alpha-galactosidase A—replacement therapy in Fabry's disease. N. Engl. J. Med. 345, 9–16.

Gimenez-Llort, L., Fernandez-Teruel, A., Escorihuela, R.M., *et al.* (2002). Mice lacking the adenosine A1 receptor are anxious and aggressive, but are normal learners with reduced muscle strength and survival rate. Eur. J. Neurosci. 16, 547–550.

Gimenez-Llort, L., Blazquez, G., Canete, T., *et al.* (2007). Modeling behavioral and neuronal symptoms of Alzheimer's disease in mice: a role for intraneuronal amyloid. Neurosci. Biobehav. Rev. 31, 125–147.

Grabowski, G.A., Leslie, N., and Wenstrup, R. (1998). Enzyme therapy for Gaucher disease: the first 5 years. Blood Rev. 12, 115–133.

Harmatz, P., Giugliani, R., Schwartz, I., *et al.* (2006). Enzyme replacement therapy for mucopolysaccharidosis VI: a phase 3, randomized, double-blind, placebo-controlled, multinational study of recombinant human N-acetylgalactosamine 4-sulfatase (recombinant human arylsulfatase B or rhASB) and follow-on, open-label extension study. J. Pediatr. 148, 533–539.

Kakkis, E.D., Muenzer, J., Tiller, G.E., *et al.* (2001). Enzyme-replacement therapy in mucopolysaccharidosis I. N. Engl. J. Med. 344, 182–188.

Keriel, A., Rene, C., Galer, C., *et al.* (2006). Canine adenovirus vectors for lung-directed gene transfer: efficacy, immune response, and duration of transgene expression using helper-dependent vectors. J. Virol. 80, 1487–1496.

Kremer, E.J., Boutin, S., Chillon, M., and Danos, O. (2000). Canine adenovirus vectors: an alternative for adenovirus-mediated gene transfer. J. Virol. 74, 505–512.

Langford-Smith, A., Wilkinson, F.L., Langford-Smith, K.J., *et al.* (2012). Hematopoietic stem cell and gene therapy corrects primary neuropathology and behavior in mucopolysaccharidosis IIIA mice. Mol. Ther. 20, 1610–1621.

Lau, A.A., Rozaklis, T., Ibanes, S., *et al.* (2012). Helper-dependent canine adenovirus vector-mediated transgene expression in a neurodegenerative lysosomal storage disorder. Gene 491, 53–57.

LeBowitz, J.H., Grubb, J.H., Maga, J.A., *et al.* (2004). Glycosylation-independent targeting enhances enzyme delivery to lysosomes and decreases storage in mucopolysaccharidosis type VII mice. Proc. Natl. Acad. Sci. USA 101, 3083–3088.

Levy, B., Galvin, N., Vogler, C., *et al.* (1996). Neuropathology of murine mucopolysaccharidosis type VII. Acta Neuropathol. 92, 562–568.

Liu, G., Martins, I., Wemmie, J.A., *et al.* (2005). Functional correction of CNS phenotypes in a lysosomal storage disease model using adeno-associated virus type 4 vectors. J. Neurosci. 25, 9321–9327.

Liu, G., Chen, Y.H., He, X., *et al.* (2007). Adeno-associated virus type 5 reduces learning deficits and restores glutamate receptor subunit levels in MPS VII mice CNS. Mol. Ther. 15, 242–247.

Lowenstein, P.R., Mandel, R.J., Xiong, W.D., *et al.* (2007). Immune responses to adenovirus and adeno-associated vectors used for gene therapy of brain diseases: the role of immunological synapses in understanding the cell biology of neuroimmune interactions. Curr. Gene Ther. 7, 347–360.

Moore, D.J., Markmann, J.F., and Deng, S. (2006). Avenues for immunomodulation and graft protection by gene therapy in transplantation. Transpl. Int. 19, 435–445.

Muenzer, J. (2011). Overview of the mucopolysaccharidoses. Rheumatology (Oxford) 50 Suppl. 5, v4–v12.

Muhammad, A.K., Xiong, W., Puntel, M., *et al.* (2012). Safety profile of gutless adenovirus vectors delivered into the normal brain parenchyma: implications for a glioma phase 1 clinical trial. Hum. Gene Ther. Methods 23, 271–284.

O'Connor, L.H., Erway, L.C., Vogler, C.A., *et al.* (1998). Enzyme replacement therapy for murine mucopolysaccharidosis type VII leads to improvements in behavior and auditory function. J. Clin. Invest. 101, 1394–1400.

Perreau, M., and Kremer, E.J. (2005). Frequency, proliferation, and activation of human memory T cells induced by a non-human adenovirus. J. Virol. 79, 14595–14605.

Perreau, M., Guerin, M.C., Drouet, C., and Kremer, E.J. (2007a). Interactions between human plasma components and a xenogenic adenovirus vector: reduced immunogenicity during gene transfer. Mol. Ther. 15, 1998–2007.

Perreau, M., Mennechet, F., Serratrice, N., *et al.* (2007b). Contrasting effects of human, canine, and hybrid adenovirus vectors on the phenotypical and functional maturation of human dendritic cells: implications for clinical efficacy. J. Virol. 81, 3272–3284.

Salinas, S., Bilsland, L.G., Henaff, D., *et al.* (2009). CAR-associated vesicular transport of an adenovirus in motor neuron axons. PLoS Pathog. 5, e1000442.

Sardiello, M., Palmieri, M., di Ronza, A., *et al.* (2009). A gene network regulating lysosomal biogenesis and function. Science 325, 473–477.

Schagen, F.H., Rademaker, H.J., Rabelink, M.J., *et al.* (2000). Ammonium sulphate precipitation of recombinant adenovirus from culture medium: an easy method to increase the total virus yield. Gene Ther. 7, 1570–1574.

Schuldt, A.J., Hampton, T.J., Chu, V., *et al.* (2004). Electrocardiographic and other cardiac anomalies in beta-glucuronidase-null mice corrected by nonablative neonatal marrow transplantation. Proc. Natl. Acad. Sci. USA 101, 603–608.

Seok, J., Warren, H.S., Cuenca, A.G., *et al.* (2013). Genomic responses in mouse models poorly mimic human inflammatory diseases. Proc. Natl. Acad. Sci. USA 110, 3507–3512.

Shipley, J.M., Klinkenberg, M., Wu, B.M., *et al.* (1993). Mutational analysis of a patient with mucopolysaccharidosis type VII, and identification of pseudogenes. Am. J. Hum. Genet. 52, 517–526.

Sly, W.S., Vogler, C., Grubb, J.H., *et al.* (2001). Active site mutant transgene confers tolerance to human beta-glucuronidase without affecting the phenotype of MPS VII mice. Proc. Natl. Acad. Sci. USA 98, 2205–2210.

Soper, B.W., Lessard, M.D., Vogler, C.A., *et al.* (2001). Nonablative neonatal marrow transplantation attenuates functional and physical defects of beta-glucuronidase deficiency. Blood 97, 1498–1504.

Sotak, B.N., Hnasko, T.S., Robinson, S., *et al.* (2005). Dysregulation of dopamine signaling in the dorsal striatum inhibits feeding. Brain Res. 1061, 88–96.

Soudais, C., Laplace-Builhe, C., Kissa, K., and Kremer, E.J. (2001). Preferential transduction of neurons by canine adenovirus vectors and their efficient retrograde transport *in vivo*. FASEB J. 15, 2283–2285.

Soudais, C., Skander, N., and Kremer, E.J. (2004). Long-term *in vivo* transduction of neurons throughout the rat CNS using novel helper-dependent CAV-2 vectors. FASEB J. 18, 391–393.

Thomas, C.E., Birkett, D., Anozie, I., *et al.* (2001). Acute direct adenoviral vector cytotoxicity and chronic, but not acute, inflammatory responses correlate with decreased vector-mediated transgene expression in the brain. Mol. Ther. 3, 36–46.

Thurberg, B.L., Lynch Maloney, C., Vaccaro, C., *et al.* (2006). Characterization of pre- and post-treatment pathology after enzyme replacement therapy for Pompe disease. Lab. Invest. 86, 1208–1220.

Vogler, C., Levy, B., Kyle, J.W., *et al.* (1994). Mucopolysaccharidosis VII: postmortem biochemical and pathological findings in a young adult with beta-glucuronidase deficiency. Mod. Pathol. 7, 132–137.

Vogler, C., Sands, M.S., Galvin, N., *et al.* (1998). Murine mucopolysaccharidosis type VII: the impact of therapies on the clinical course and pathology in a murine model of lysosomal storage disease. J. Inherit. Metab. Dis. 21, 575–586.

Wilcox, W.R., Banikazemi, M., Guffon, N., *et al.* (2004). Long-term safety and efficacy of enzyme replacement therapy for Fabry disease. Am. J. Hum. Genet. 75, 65–74.

Address correspondence to:
*Dr. Assumpció Bosch*
*CBATEG, Edifici H*
*Campus Universitat Autònoma de Barcelona*
*08193 Bellaterra, Barcelona*
*Spain*

*E-mail:* assumpcio.bosch@uab.es

Received for publication August 6, 2013;
accepted after revision November 19, 2013.

Published online: December 3, 2013.